CORROSION BEHAVIOR OF STAINLESS STEEL CLAD REBAR

Fushuang Cui, A.A. Sagüés
Dept. of Civil and Environmental Engineering, College of Engineering
University of South Florida
4202 E. Fowler Ave., Tampa, Florida 33620

Rodney G. Powers
Materials Office
Florida Department of Transportation
2006 N.E. Waldo Rd.
Gainesville, Florida 32609

ABSTRACT

Stainless steel clad rebar (SCR) was investigated because it may become a cost-effective means of controlling corrosion in concrete under very aggressive environments. Sound SCR (316L cladding) resisted corrosion in saturated $Ca(OH)_2$ solution (SCS) with up to 5 wt% chloride. Cladding breaks on SCR induced significant corrosion of exposed underlying CS in SCS with only 1 wt% chloride. A computer model using laboratory data as input was constructed to evaluate the extent of galvanic corrosion of SCR. Modeling indicated that concrete resistivity and size of the cladding break are the main controlling factors of galvanic corrosion.

Keywords: stainless steel clad rebar, galvanic, corrosion, chloride, potential, concrete

INTRODUCTION

Austenitic stainless steel (SS) rebars have shown very promising corrosion performance in chloride-contaminated concrete [1-6] but at a higher cost than conventional plain carbon steel (CS) rebar. Stainless steel clad rebar (SCR) [7] with a carbon steel core offers the potential for performance comparable to that of solid SS rebar but at a much lower cost. However, SCR is vulnerable to corrosion at cladding breaks such as may result from local mechanical damage or unprotected cut ends. Upon chloride contamination of the surrounding concrete an intense galvanic couple may develop between the anodic exposed carbon steel and the surrounding, still passive, stainless steel. These conditions can be especially promoted in marine service [8,9]. The resulting extent of corrosion is a function of the amount of base steel exposed and surrounding stainless steel, the polarization characteristics of both, and the properties of the surrounding concrete.

This work examined these issues by characterizing the corrosion behavior of SCR in the sound condition (no cladding breaks), and with intentionally introduced breaks, in a saturated $Ca(OH)_2$ solution (SCS) to which controlled amounts of chloride ion were added. The results were input to a simplified model to estimate the extent of corrosion that may result from the corrosion macrocell between a small spot of carbon steel exposed at a cladding break and the rest of a reinforced concrete assembly.

EXPERIMENTAL

The SCR was size No. 5 (16 mm diameter), corrugated, with a 0.8 mm thick cladding of Type 316L SS, and manufactured in a regular production run using the Nuovinox process [7].

The SCR specimens were 10 cm long and prepared in the configuration types A, B and C shown in Figure 1. The rebar surface was sandblasted before preparing the specimens. Types A and C had sound (no breaks) cladding, while Type B had a single 4-mm diameter hole near the middle, drilled so the full diameter of the bit just penetrated the entire cladding thickness exposing a shallow conical CS surface. Type C were creviced specimens consisting of two touching bars tightly tied with Type 316L SS wire (0.79 mm diameter) which also served as the external electric contact. Electric contact to Types A and C was made through copper wires placed at the ends. All SCR cut ends (and copper wire contacts) were embedded in metallographic epoxy compound caps.

The SCS test media were prepared by adding 2 g/l $Ca(OH)_2$ to distilled water, resulting in pH ~12.6. Reagent grade NaCl was used as the Cl^- source. A saturated calomel electrode (SCE) was used as the reference electrode, and a high density graphite rod was used as counter electrode. All tests were performed at room temperature, 22±1C, and under naturally aerated conditions.

Type A SCR specimens were tested immersed in SCS and SCS with 5 wt% Cl^-, and Type B specimens were tested in SCS with 1 wt% Cl^-. Type C SCR specimens were exposed to SCS to which NaCl was added stepwise every 7 days until reaching a Cl^- concentration of 8 wt%. The open circuit potential E_{oc} (OCP) and electrochemical impedance spectroscopy (EIS) responses were monitored periodically during the test exposures. The EIS frequency range was from 100 kHz to 1 mHz (10 mHz for type B specimens). The equivalent circuit fitting parameters shown in Figure 2 were used to fit all the EIS spectra and obtain Rp, Rs, Yo and n. The value of Rp was used to calculate a nominal corrosion current density i_{ncorr}=0.026 V/Rp [10].

RESULTS AND DISCUSSION

Solution Tests

Experiments were performed on duplicate specimens and the behavior described below was found to be reproducible.

Figures 3 and 4 shows E_{oc} and i_{ncorr} as function of time for sound SCR (Type A) in SCS and SCS with 5 wt%. Starting from less than -0.33 V, E_{oc} of all samples tended to stabilize at around ~-0.2 V. While E_{oc} increased, corrosion rate decreased rapidly to less than 0.1 $\mu A/cm^2$, indicative of a passive film that became increasingly mature with time. By combining all the E_{oc} and i_{ncorr} data (Figure 5), an apparent cathodic Tafel slope of ~ 0.130 V/dec was obtained.

While sound SCR was passive in SCS with 5 wt% Cl^-, SCR with a 4-mm diameter cladding break (Type B) corroded rapidly in SCS with 1 wt% Cl^- and corrosion products covered the hole after a few days exposure. Figure 6 shows typical Nyquist diagrams of SCR both sound and with a cladding break in SCS with 1 wt% Cl^- (after 16-hour immersion). The Rp values computed from these curves considering the entire surface are 438 $k\Omega.cm^2$ (sound) and 18.1 $k\Omega.cm^2$ (with a cladding break). The corresponding open circuit potential E_{oc} was -0.26 V and -0.506 V respectively. If only the area of the exposed CS is considered, the specific Rp for the cladding break is 0.05 $k\Omega.cm^2$, yielding a local i_{ncorr} value of 510 $\mu A/cm^2$. These results are consistent with the observation of corrosion when the underlying carbon steel was exposed.

The E_{oc} of type C specimens of SCR in SCS, shown in Figure 7, initially increased with time even though the Cl^- concentration was increasing up to 5 wt%. E_{oc} of SCR did decrease when more Cl^- was added, but coinciding with the observation of crevice corrosion at the junction with the epoxy caps. The freely exposed surface of the SCR did not show any corrosion products. The performance of SCR in these tests is comparable to that reported elsewhere for solid SS bar [(11)].

While sound SCR showed high corrosion resistance, SCR with a cladding break was susceptible to significant corrosion. Once corrosion of exposed CS starts, a galvanic corrosion cell forms by coupling with the passive stainless steel clad which can sustain appreciable cathodic current. Because the cathode/anode ratio in concrete structures is expected to be large, galvanic corrosion of SCR could be important. To investigate the possible extent of corrosion, a preliminary model calculation was performed.

MODELING

The modeling estimates the amount of corrosion that could develop at a spot on the SCR where a small cladding break exists. This break could represent, for example, a small residual flaw where a weld overlay failed to completely cover a rebar cut end. This model is a modified version of a similar approach used to study corrosion distribution in rebar assemblies [(12)].

Definitions and Assumptions

The cladding break is idealized as a round opening of radius r_o at an otherwise clad overlayed end of a rebar. The CS is assumed to be already undercut by some corrosion so that affected region is twice the size of the clad break (area of carbon steel 4 times that of the break).

Macrocell coupling between the anodic spot and the cathodic SS surfaces takes place with the immediately surrounding region (mm scale), nearby surfaces (cm-dm scale), and with the rest of the entire rebar assembly (m scale). The effects of the latter were explored first as very large cathodic areas can be involved.

The structural element considered (Figure 8) is a column with height H and diameter D. For computation, the column is divided into slices of thickness L. N rebars are placed longitudinally around the circumference of the column with transverse circular hoops spaced a distance L from each other. All the rebars have radius r_r. The rebar cover is C, considered for simplicity to be the same for longitudinal and hoop bars. The rebar cage is electrically continuous. For a worst-case coupling condition, it is assumed that there is only one clad break in the entire column, at one of the bar ends near an end of the column. The concrete is assumed to have constant resistivity ρ.

The CS exposed by the clad break is assumed to be in the active condition, due to chloride contamination of the adjacent concrete. The SS is assumed to be passive everywhere. The corrosion current density i_{corr} of the CS is assumed to be given by

$$i_{corr} = i_{oa}\, 10^{\wedge}[(E_{cs} - E_{oa})/\beta_a] \qquad (1)$$

and net cathodic current on the SS is assumed to be given by

$$i_c = i_{oc}\, 10^{\wedge}[(E_{oc} - E_{ss})/\beta_c] - i_p \qquad (2)$$

so that both CS anodic and SS cathodic processes are assumed to be determined by Butler-Volmer kinetics, with no diffusional polarization, and with Tafel slopes β_a and β_c, exchange current densities i_{oa} and i_{oc}, equilibrium potentials E_{oa} and E_{oc} and local electrode potentials E_{cs} and E_{ss}. A passive dissolution current density i_p is assumed for the SS. All magnitudes are assigned appropriate sign as needed.

The undercut beneath the clad break is conservatively assumed to contain non-protective corrosion products, and electrolyte with negligible electric resistance. The clad break is electrolytically coupled with the rest of the structure through the intervening concrete. The Ohmic resistance to the immediately surrounding concrete is approximated by that of a disk of radius r_o facing a semi-infinite medium [13]:

$$Ro = \rho/4r_o \qquad (3)$$

The subsequent electrolytic coupling between the region surrounding the anode and the rest of the column is approximated by a one-dimensional model that has longitudinal resistance per column slice given by

$$R = \rho L/\pi r_c^2 \qquad (4)$$

and lateral resistance

$$RL = \left[\left(\frac{\rho}{2\pi LN} \ln\left(\frac{C}{r_r}\right) \right)^{-1} + \left(\frac{\rho}{4\pi^2 (r_c - C)} \ln\left(\frac{C}{r_r}\right) \right)^{-1} \right]^{-1} \qquad (5)$$

For the lateral resistance it is assumed that the resistance for each of the longitudinal and hoop rebars is the same as the radial resistance of a concrete cylinder of outer radius C and inner radius r_r, centered on the rebar, and with length equal to the length of the rebar in the column slice of length L [(14)]. All the lateral rebar resistances within a slice are considered to be in parallel.

The model described above corresponds to an equivalent circuit with one anodic voltage source and H/L net cathodic voltage sources arranged in a truncated transmission line. The inputs to the model consist of the polarization parameters for the corrosion reactions described in Eqs. (1) and (2), geometric parameters (the column dimensions, number and diameter of rebars, imperfection radius), and resistivity of concrete. The model output is the corrosion current at the imperfection (main goal of the modeling calculation), and the cathodic current at each slice. Potentials at each node of the equivalent circuit can be also calculated from the output.

The polarization parameters, summarized in Table 1, have been abstracted from the experimental results given earlier. For the anodic reaction a nominal Tafel slope of 0.06 V/dec was assumed. The i_{oa} value was then adjusted to obtain a corrosion current matching that estimated from the EIS tests (at the appropriate potential). A nominal passive current density $i_p=10^{-3}$ $\mu A/cm^2$ was also assumed. This value, combined with the choice of cathodic polarization parameters, yields an undisturbed E_{oc}=-0.03 V for the SS (roughly approximating the experimental values).

The base case was chosen to represent a typical marine substructure reinforced concrete column arrangement, with high quality concrete and a small clad break. The input parameters were: L=30 cm, $D=2r_c$=100 cm, N=10, r_r=0.79 cm, C=10 cm, ρ=30 kΩ.cm and r_o=0.05 cm. Calculations using other values of r_o and ρ were also performed to examine the sensitivity of corrosion to these two factors.

Calculation Results and Discussion

The calculation output for the base condition is given in Figure 9. The cathodic current, as expected, decreased but slowly with distance to anode, while the potential of cathodes (much higher than the anode potential) changed little. These trends indicated that much of the resistive potential drop took place near the clad break. The anodic current was only a few μA, but concentrated in the area of the clad break. For the purpose of estimating the time to crack the concrete cover, the corrosion product

accumulation was assumed to act on the entire face of the overlayed rebar cut end that contains the break. Thus, an effective corrosion current density i_{eff} was defined as $I_a/\pi r_r^2$. Figure 10 summarizes calculation results with different values of cladding break size r_o and concrete resistivity ρ. Clearly, when the size of r_o increased or ρ decreased, i_{eff} increased rapidly.

For the system and parameters chosen here, galvanic corrosion was resistance-controlled, and R_o was the most important resistive term (consistent with the current and potential trends noted above). Since $R_o = \rho/4r_o$, the break size r_o and concrete resistivity ρ are critical to the outcome. From Figure 10, the dependence of i_{eff} on those parameters may be approximated by

$$i_{eff} = k\, r_o/\rho^{0.9} \qquad (6)$$

where i_{eff} is in $\mu A/cm^2$, r_o is in cm, ρ is in $k\Omega.cm$, and k=720 (for the chosen units) for this system.

Additional calculations showed that the results were nearly insensitive to the assumed size of the CS area undercut beneath the break.

As indicated earlier, the above calculations ignored the coupling between the anodic spot and the SS immediately surrounding it in a mm size scale. Preliminary calculations based on solutions to the disk-on-plane problem [15] suggest that short-distance coupling could fractionally increase the overall macrocell current estimated above. Modeling to address this issue is in progress.

Exploratory calculations were also conducted to examine the effect of coupling with only a short (e.g. 30 cm) length of SS rebar near the clad break. Consistent with the previous finding of the importance of R_o, the results indicated that at moderate to high concrete resistivities much of the coupling effect could be contributed by this region. Thus, a treatment involving an entire structural element may not be needed in most cases. This modeling effort is in progress to address other conditions and clad break configurations.

Service Life Implications

The service life T of a reinforced concrete structure is often estimated using the general approach proposed by Tuutti [16]:

$$T = T_1 + T_2 \qquad (7)$$

where T_1 is the corrosion initiation time and T_2 is the corrosion propagation time (from initiation until cracking of the concrete cover).

The end of the propagation period is reached when a critical accumulation of corrosion products (equivalent to a critical corrosion penetration X_{crit}) develops at the rebar surface. Recent work [17] has shown that when corrosion is restricted to a small length of rebar, X_{crit} can be estimated using the following empirical equation:

$$X_{crit} \sim 0.011 \cdot \left(\frac{C}{\phi}\right) \cdot \left(\frac{C}{L_c} + 1\right)^{1.8} \quad \text{(mm)} \qquad (8)$$

where C is the concrete cover thickness, ϕ is rebar diameter and L_c is length of the corroding rebar section.

A rough estimate of T_2 may be made by assuming that Eq. (8) also applies when L_c is substituted by $2r_r$, the characteristic length of the corrosion expansion section considered here (the overlayed cut end). Moreover, X_{crit} can be related to i_{eff} and T_2 by Faradaic conversion so that

$$T_2 = \frac{2F\rho_S X_{crit}}{i_{eff} A_W} \qquad (9)$$

where F is Faraday's constant, ρ_S and A_W are the density and atomic weight of iron, which is assumed to corrode as divalent cations.

Application of Eq. (8) to the base case (No.5 rebar, C=10 cm, $\phi = L_c = 1.58$ cm and $r_o = 0.05$ cm) yields $X_{crit} \sim 2.5$ mm. This value is only nominal as it involves extrapolation beyond the range of conditions used to develop Eq. (8). Nevertheless, the large estimated X_{crit} reflects the mitigating effect of limiting corrosion to a relatively small area beneath a thick concrete cover [17]. For the base case with high quality concrete of ρ=30 kΩ.cm, Eqs (6) and (9) project T_2 > 100 years. This good prognosis derates rapidly if r_o increases or ρ decreases. Thus, tolerance to a cladding break appears promising as long as the break is small (e.g. <1 mm diameter) and the concrete resistivity is high.

The above analysis is preliminary in nature and needs to be followed by detailed characterization of the corrosion behavior of SCR in actual concrete service. Moreover, the modeling approach used was highly simplified and additional refinement of the underlying assumptions (notably incorporation of short range coupling between the break and the immediately surrounding steel) and solution methods is needed in future work. Issues such as the nature of the occluded chemistry beneath the break, and potential beneficial effects of corrosion product plugging of the break merit further consideration. Corrosion product-induced changes in concrete resistivity around the break, which may significantly affect the extent of macrocell coupling, should also be examined. Finally, the projection to obtain X_{crit} involved large extrapolation and assumed that the accumulation of corrosion products in the present case roughly corresponded to that used to formulate Eq. (8); the validity of this approach needs to be further investigated.

CONCLUSIONS

1. Sound SCR had high corrosion resistance in liquid solution tests, comparable to that reported for solid SS bars.
2. Cladding breaks on SCR resulted in localized corrosion development.
3. The corrosion rate of exposed CS in SCR depended highly on resistivity of concrete and clad break size. Better quality (higher resistivity) concrete and smaller imperfection sizes on SCR were projected to significantly reduce corrosion.

4. Preliminary model calculations suggested that widely spaced cladding breaks of sub-millimeter size would be tolerable in concrete that retains high resistivity.

ACKNOWLEDGEMENT

This work was supported by Stelax (U.K.) Limited. and in cooperation with the Florida Department of Transportation. The findings and opinions expressed in this paper are those of the authors and not necessarily those of the supporting organizations.

REFERENCES

1. G.N. Flint, R.N. Cox, Magazine of Concrete Research 40, 142 (March 1988): p.13.

2. R.N. Cox, J.W. Oldfield, "The Long Term Performance of Austenitic Stainless Steel in Chloride Contaminated Concrete," Proceedings of the Fourth International Symposium on Corrosion of Reinforcement in Concrete Construction, Eds. C.L. Page, P.B. Bamforth and J.W. Figg, (Cambridge, UK: Society of Chemical Industry, 1996), p. 662.

3. U. Nurnberger, "Corrosion Behavior of Welded Stainless Steel Reinforced Steel in Concrete," Proceedings of the Fourth International Symposium on Corrosion of Reinforcement in Concrete Construction, Eds. C.L. Page, P.B. Bamforth and J.W. Figg, (Cambridge, UK: Society of Chemical Industry, 1996), p. 623.

4. P. Pedeferri, L. Bertolini, F. Bolzoni, T. Pastore, "Behavior of Stainless Steels in Concrete," Proceedings of the International Seminar: The State of the Art of the Repair and Rehabilitation of Reinforced Concrete Structures Eds. W.F. Silva-Araya, O.T. DE RINCÓN, and L. P. O'Neill, (Reston, VA: ASCE, 1997): p.192.

5. D.B. McDonald, D.W. Pfeifer, M.R. Sherman, "Corrosion Evaluation of Epoxy-Coated, Metallic-Clad and Solid Metallic Reinforcing Bars in Concrete," U.S. Dpt. of Transportation: Federal Highway Administration Report, Publication No. FHWA-RD-98-153, 1998

6. J. Hewitt, M.Tullmin, "Corrosion and Stress Corrosion Cracking Performance of Stainless Steel and Other Reinforcing Bar Materials in Concrete," Proceedings of International Conference: Corrosion and Corrosion Protection of Steel in Concrete, Ed. K. N. Swamy, (Sheffield, UK: Sheffield Academic Press, 1994): p. 527.

7. NUOVINOX, Product Information, (West Glamorgan, U.K.: Stelax (U.K.) Limited, 1998)

8. A. Zayed, A. Sagüés, R. Powers, "Corrosion of epoxy-coated reinforcing steel in concrete," Corrosion/89, paper No. 379, (Houston, TX: NACE International, 1989)

9. A. Zayed, A. Sagüés, Corrosion Science 30, 10 (1990): p. 1025.

10. D.A. Jones, Principles and Prevention of Corrosion, (New York: Macmillan Publishing Company, 1992): p. 147.

11. L. Bertolini, F. Bolzoni, T. Pastore, P. Pedeferri, British Corrosion Journal 31, 3(1996): p. 218.

12. A. Sagüés, H. M Perez-Duran, R. Powers, Corrosion 47, 11 (1991): p. 884.

13. R. Oltra, M. Keddam, Corrosion Science 28, 1 (1988): p. 1.

14. A. Bentur, S. Diamond, N.S. Berke, Steel Corrosion in Concrete, (London, U.K.: E&FN Spon, 1997): p. 85.

15. W. Smyrl, J. Newman, J. Electrochem. Soc., 123 (1976): p. 1423.

16. K. Tuutti, Corrosion of Steel in Concrete, (Stockholm, Sweden: Swedish Cement and Concrete Research Institute, S-100 44, 1982)

17. A.A. Torres-Acosta, A. Sagüés, "Concrete Cover Cracking with Localized Corrosion of Reinforcing Steel," Proceedings of the 5th CANMET/ACI International Conference on Durability of Concrete, SP-192, Ed. V.M. Malhotra, (Farmington Hills, Mich: American Concrete Institute, 2000): p. 591.

TABLE 1
POLARIZATION PARAMETERS CHOSEN FOR THE CALCULATIONS

	$E_{oa,c}$ (V vs SCE)	$i_{oa,c}$ ($\mu A/cm^2$)	$\beta_{a,c}$ (V/dec)
Anodic	-0.866	$5.1 \cdot 10^{-4}$	0.06
Cathodic	0.23	$1 \cdot 10^{-5}$	0.13

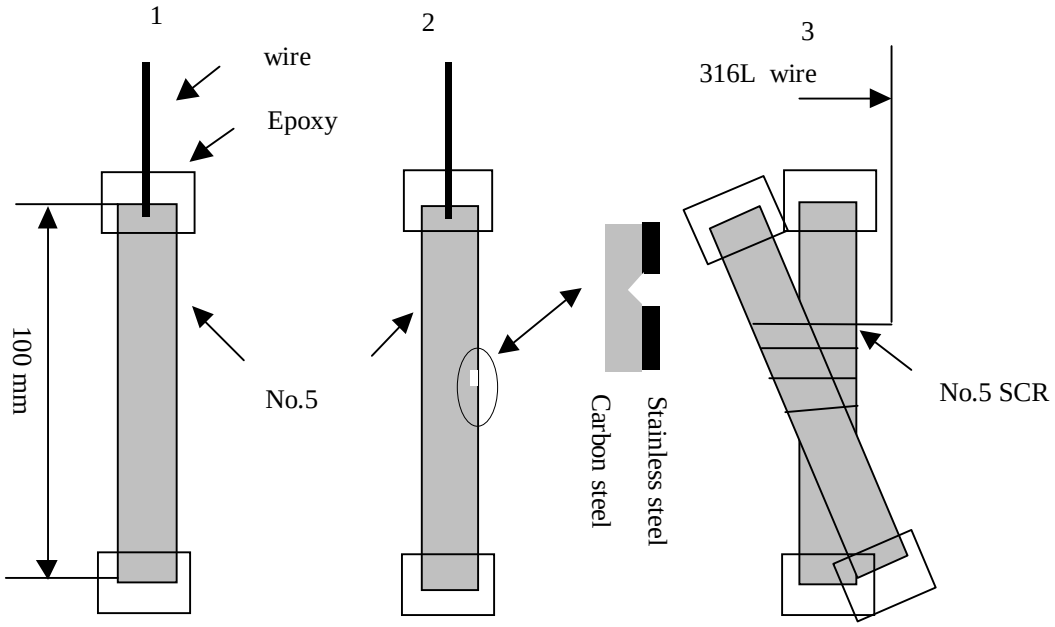

FIGURE 1 - Rebar specimens used in solution tests: 1 type A SCR; 2. type B SCR; 3. type C SCR

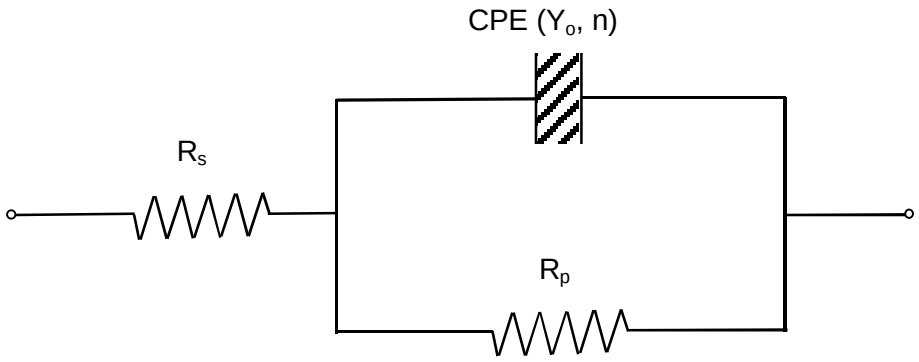

Rs: solution resistance
Rp: polarization resistance
CPE: constant phase-angle element ($Z=Y_o^{-1}(j\omega)^{-n}$)

FIGURE 2 - Equivalent circuit used to interpret the EIS results

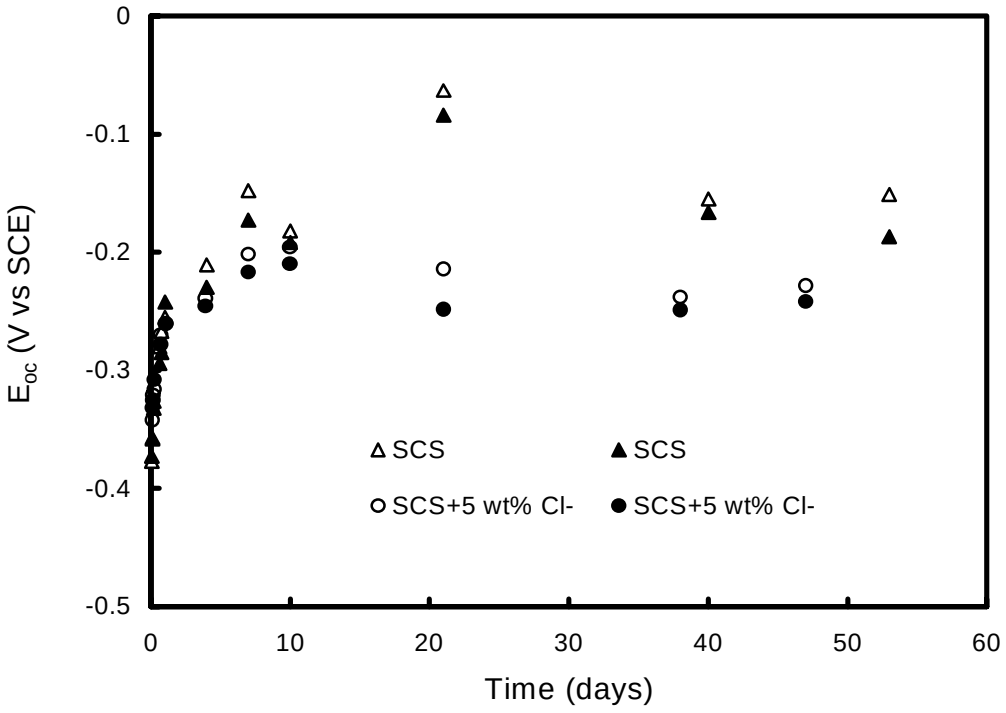

FIGURE 3 - E_{oc} of sound SCR in naturally aerated SCS

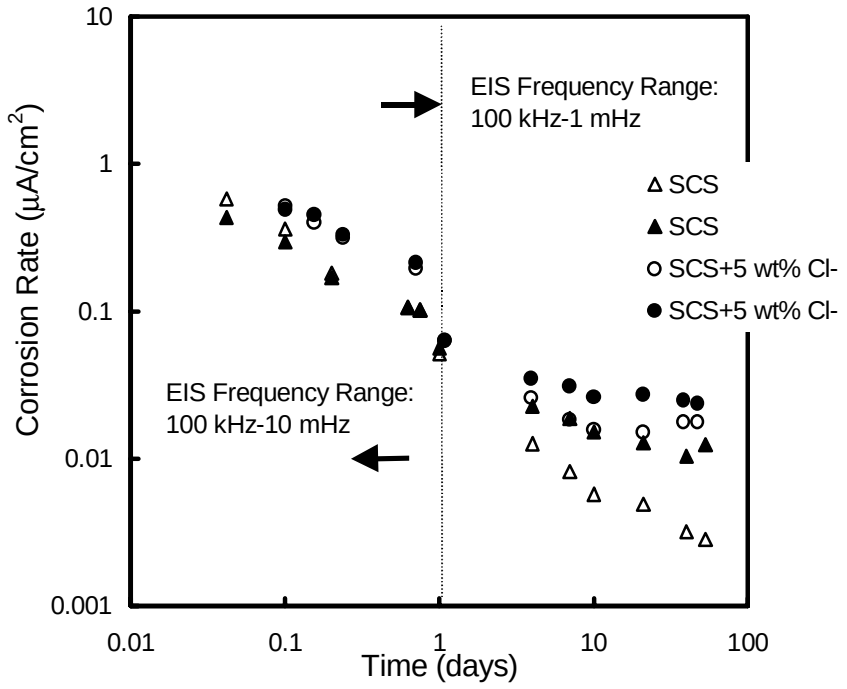

FIGURE 4 - Corrosion rate of sound SCR in naturally aerated SCS

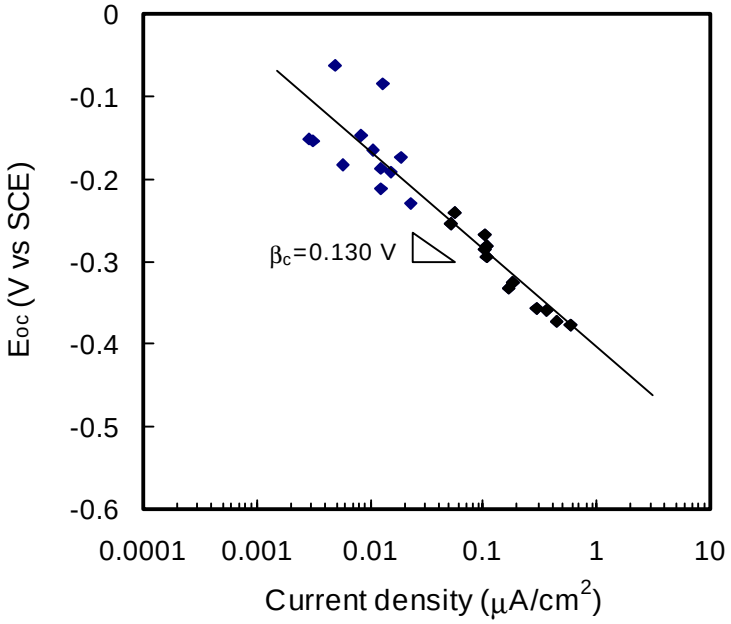

FIGURE 5 - Corrosion behavior of sound SCR in naturally aerated SCS

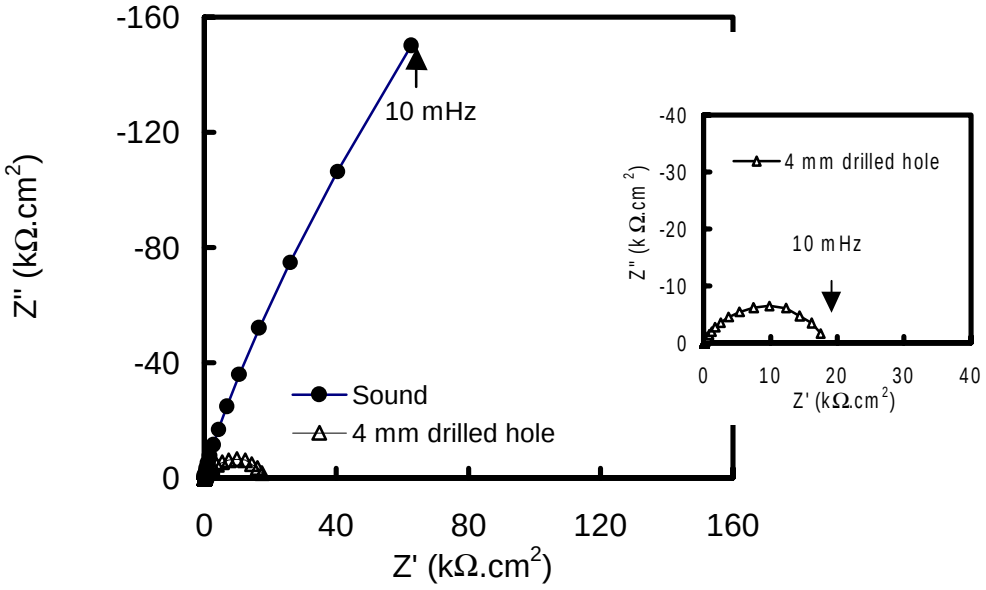

FIGURE 6 - Effect of imperfections on corrosion behavior of SCR in naturally aerated SCS with 1 wt% Cl^-

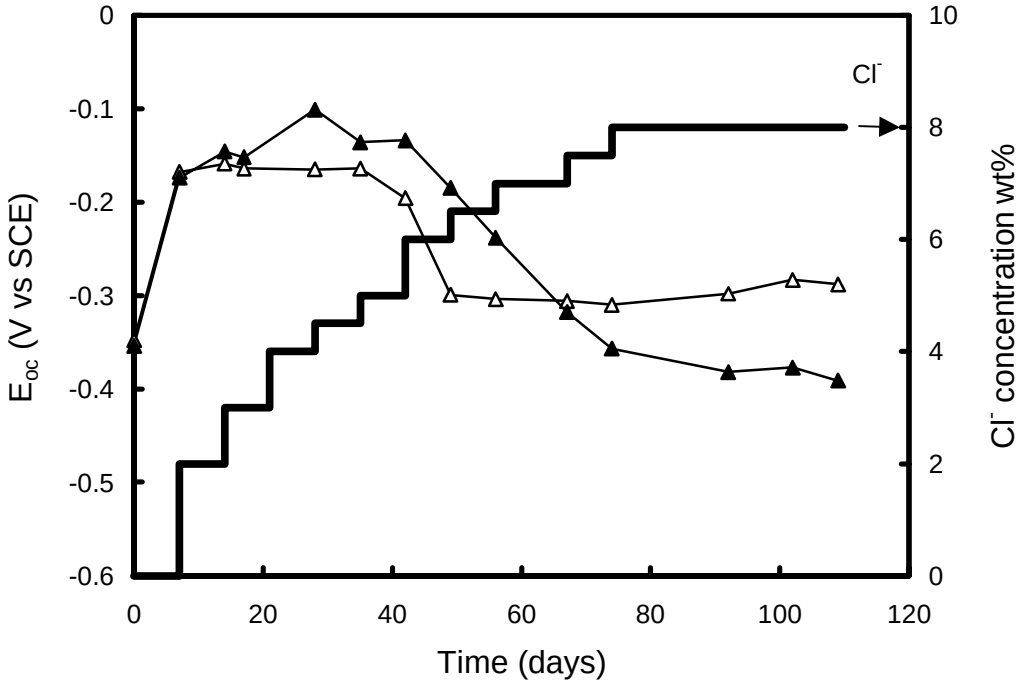

FIGURE 7. E_{oc} of sound SCR in naturally aerated SCS

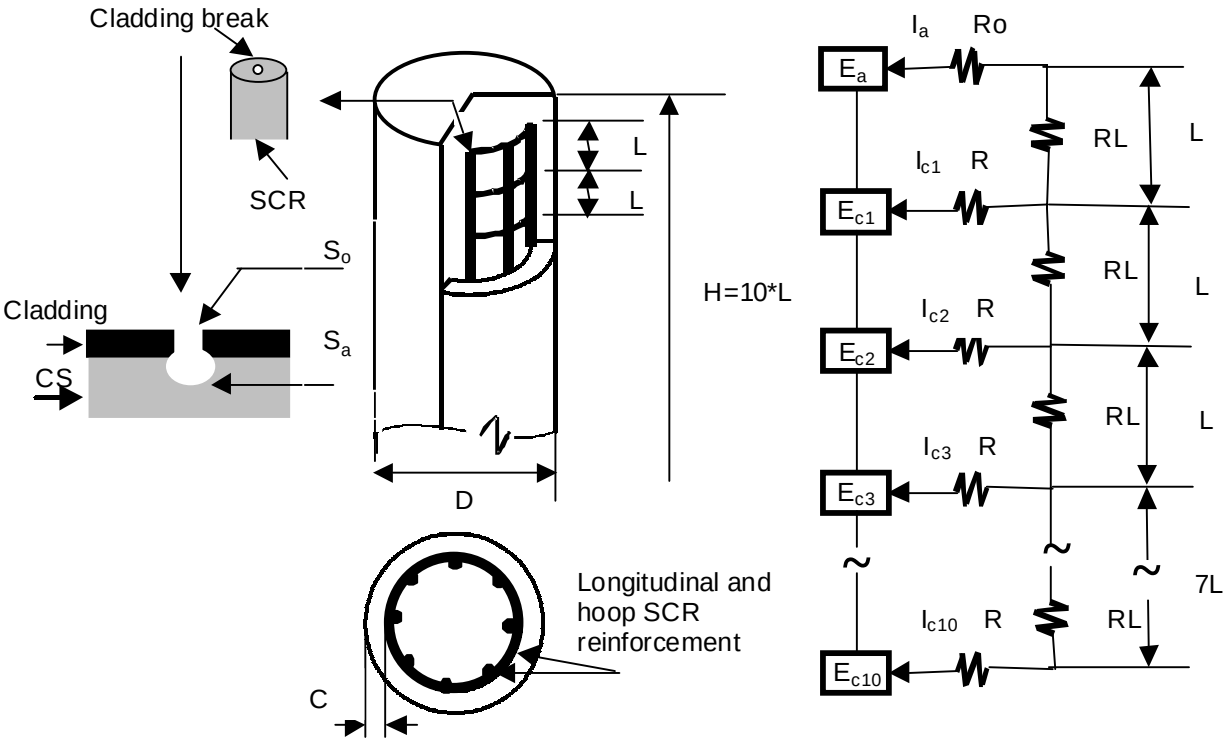

FIGURE 8 - Schematic of concrete column, equivalent circuit, and cladding break

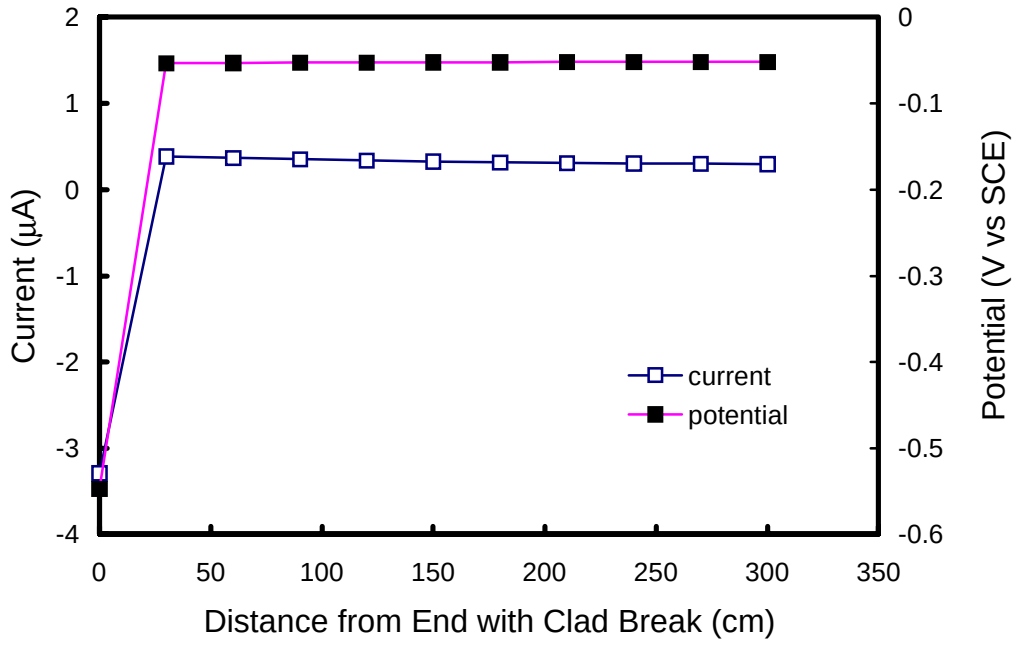

FIGURE 9 - Model output: current per segment (anode: negative) and potential distribution

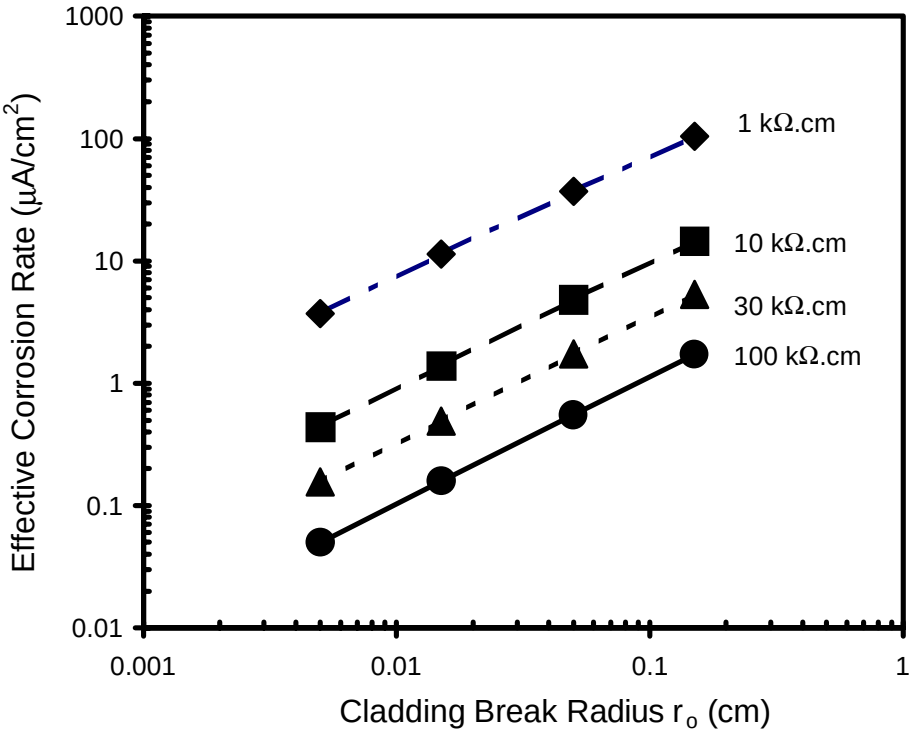

FIGURE 10 - Model output: corrosion sensitivity to clad break size and concrete resistivity